

www.acsami.org Research Article

Empirical Optimization of Peptide Sequence and Nanoparticle Colloidal Stability: The Impact of Surface Ligands and Implications for Colorimetric Sensing

Zhicheng Jin, Justin Yeung, Jiajing Zhou, Maurice Retout, Wonjun Yim, Pavla Fajtová, Bryan Gosselin, Ivan Jabin, Gilles Bruylants, Hedi Mattoussi, Anthony J. O'Donoghue, and Jesse V. Jokerst*



Cite This: ACS Appl. Mater. Interfaces 2023, 15, 20483-20494



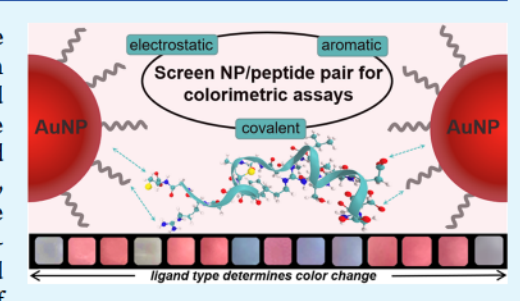
ACCESS

Metrics & More

Article Recommendations

Supporting Information

ABSTRACT: Surface ligands play a critical role in controlling and defining the properties of colloidal nanocrystals. These aspects have been exploited to design nanoparticle aggregation-based colorimetric sensors. Here, we coated 13-nm gold nanoparticles (AuNPs) with a large library of ligands (e.g., from labile monodentate monomers to multicoordinating macromolecules) and evaluated their aggregation propensity in the presence of three peptides containing charged, thiolate, or aromatic amino acids. Our results show that AuNPs coated with the polyphenols and sulfonated phosphine ligands were good choices for electrostatic-based aggregation. AuNPs capped with citrate and labile-binding polymers worked well for dithiol-bridging and π - π stacking-induced aggregation. In the example of



electrostatic-based assays, we stress that good sensing performance requires aggregating peptides of low charge valence paired with charged NPs with weak stability and *vice versa*. We then present a modular peptide containing versatile aggregating residues to agglomerate a variety of ligated AuNPs for colorimetric detection of the coronavirus main protease. Enzymatic cleavage liberates the peptide segment, which in turn triggers NP agglomeration and thus rapid color changes in <10 min. The protease detection limit is 2.5 nM.

KEYWORDS: surface ligand, colorimetric sensor, inorganic nanocrystal, peptide design, nanoparticle aggregation, main protease

1. INTRODUCTION

The aggregation of metallic colloids leads to a bathochromic shift in their surface plasmon resonance (SPR) band and results in a pronounced color change. The ultimate color formation is a function of the core composition, particle morphology, and surface chemistry, which modulate the resonant coupling of light and free electrons in metallic nanostructures. For instance, the aggregation of gold nanoparticles (AuNPs) dramatically changes the dispersion color visually from red to purple/blue by the naked eye due to the strong sensitivity of SPR to the interparticle distance combined with the high molar absorption coefficients. Such aggregation-induced plasmonic coupling has been exploited as an optical signal transduction strategy in colorimetric sensors with widespread use in bioanalytical applications.

The realization of plasmonic coupling broadly demands either chemical linking (e.g., S-Au bond, 15,16 conjugation, 17 recognition interactions, 18,19 etc.) or changes in the environment (e.g., ionic strength, 20 solvent polarity, 21 ligand hydrophilicity, 22 etc.). Over the past two years, our group has designed a set of colorimetric sensors to study proteases through an array of NP types, proteases, and aggregation mechanisms. 5,6,16,23-26 However, we have not yet systemati-

cally investigated the effects of surface chemistry. Surface chemistry plays a critical role in endowing colloidal stability and interfacial functionality—these factors determine how nanoparticles adapt to the chemical or environmental stimuli and thus manifest in interparticle crosslinking and colorimetric sensing. The depth and diversity of the ligand field provide choices spanning from metal complexes, small organic compounds, polymers, polymers, small organic compounds, polymers, small organic compounds, polymers, small of oligonucleotides lecules (e.g., peptides, logical proteins, doligonucleotides and biological systems. Modifying surfaces with ligands allows us to tune interparticle interactions, such as the Coulombic and hydrophobic interactions, hydrogen and covalent bonds, or combinations thereof. Clearly, it is beneficial to screen the optimally desired ligands to improve the performance of

Received: January 18, 2023 Accepted: April 4, 2023 Published: April 14, 2023





Increasing [protease]

hydrophilic cleavage aggregating domain

b. This study: Ligands of different size, charge, anchor, etc.

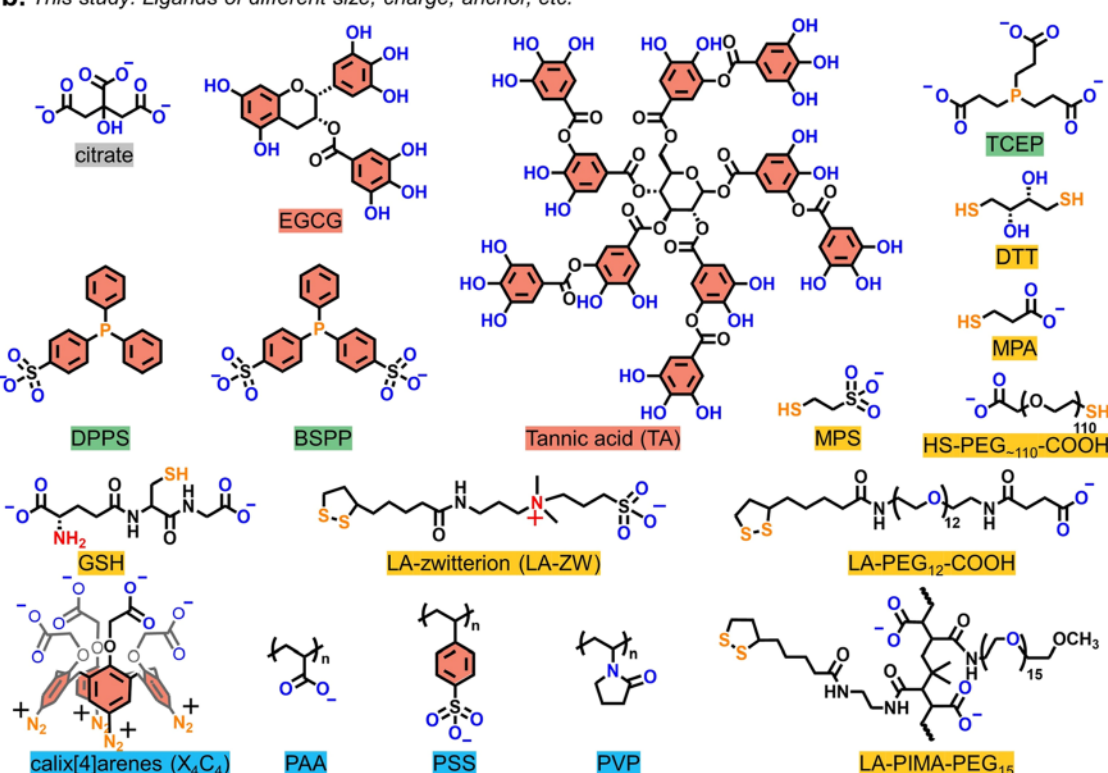


Figure 1. (a) Thematic illustration of how surface ligands on AuNPs trigger aggregation following incubation with proteolytically cleaved peptide where the Arg, Phe, and/or Cys amino acids in the peptide segments promote interparticle association via charge neutralization, $\pi-\pi$ stacking, or disulfide-bridge formation, respectively. This leads to pronounced color changes as a function of protease concentration [see the inset in part (iii)]. (b) Structure of the ligands used in this study including polyphenols (names in red), phosphine (green), thiolate (yellow), and other macromolecular ligands (blue). Note that the aryldiazonium groups in calix[4]arene (X_4C_4) are reduced in aryl radicals that form Au–C bonds with the gold surface. BSA structure is not included. In the chemical structures, the solubilizing block is coded in blue/red atoms and the anchoring group is coded in yellow/blue atoms.

aggregation-based sensors and explain the diverse interactions between NPs and aggregants.

Here, citrate-AuNPs were first derivatized with a library of 19 ligands ranging from labile molecules to multicoordinating macromolecules, thus yielding NPs with varying physiochemical properties. The colloidal stability and color changes initiated by favorable electrostatic, covalent, and hydrophobic conditions were then evaluated using NaCl and dithiothreitol (DTT), and amphiphilic peptide solutions. Our results showed that the surface ligand plays a critical role in defining the critical coagulation concentration (CCC), aggregation mechanism, and color patterns. Consequently, this allowed us to screen the optimal NP coating and rationally develop a versatile peptide that contained charged, thiolate-presenting, and aromatic amino acid residues (i.e., Arg, Cys, Phe) that

rapidly induce colorimetric signals. We finally validated the sensing performance targeting SARS-CoV-2 main protease with a detection limit of 2.5 nM and demonstrated its good performance in complex matrices including saliva. The results can facilitate new NP modifications for plasmonic sensing.

2. RESULTS AND DISCUSSION

2.1. Rationale. Evaluating the effects of surface chemistry on NP aggregation-based colorimetric sensors was motivated by the desire to improve their performance, *e.g.*, working window, sensitivity, *etc.* A second goal was to provide better understanding of the diverse interplays between NPs and aggregants (here, peptides). This was also inspired by our experimental observations relating to the different aggregation propensity of several NPs in the presence of the same

Table 1. Hydrodynamic Size $(D_{\rm H})$, Zeta Potential (ξ) , and Critical Coagulation Concentration $({\rm CCC})^a$ for the Various Ligand-Stabilized AuNPs

ligand type	sample	D_{H} (nm)	PDI	Zeta ζ (mV)	NaCl test (mM)	DTT test (μM)	FFPC test (μM)
native	citrate-Au	18.2	0.216	-30.4 ± 2.7	>50	2-100	>10
polyphenols	EGCG-Au	24.4	0.207	-30.2 ± 1.7	>500	5-50	$N.D.^c$
	TA-Au	21.0	0.270	-35.2 ± 2.9	>100	5-100	N.D.
phosphine ligands	TCEP-Au	21.0	0.284	-34.9 ± 3.0	>500	2-20	>50
	DPPS-Au	18.2	0.182	-25.2 ± 0.3	>50	N.D.	N.D.
	BSPP-Au	18.2	0.223	-31.3 ± 1.8	>100	N.D.	N.D.
thiolate ligands	DTT-Au	24.4	0.147	-41.8 ± 0.2	>50	N.D.	>200
	MPA-Au	21.0	0.168	-30.6 ± 1.0	>50	N.D.	N.D.
	MPS-Au	24.4	0.280	-46.1 ± 0.6	>50	N.D.	N.D.
	GSH-Au	18.4	0.053	-35.6 ± 2.7	>200	N.D.	N.D.
	HS-PEG _{~110} -COOH-Au	24.4	0.048	-36.4 ± 3.8	N.D.	N.D.	N.D.
	LA-PEG ₁₂ -COOH-Au	21.0	0.194	-31.2 ± 1.7	N.D.	N.D.	N.D.
	LA-ZW-Au	21.0	0.117	-26.6 ± 1.8	N.D.	N.D.	N.D.
macromolecular ligands	X ₄ C ₄ -Au	43.8	0.576	-31.6 ± 2.8	>200	N.D.	N.D.
	PAA-Au	37.8	0.162	-46.8 ± 0.4	>100	2-100	N.D.
	PSS-Au	21.0	0.423	-41.5 ± 0.7	>50	2-100	>10
	PVP-Au	24.4	0.044	-11.8 ± 0.8	N.D.	5-100	>20
	LA-PIMA-PEG ₁₅ -Au	28.2	0.225	-31.2 ± 1.7	N.D.	N.D.	N.D.
	BSA-Au	50.7	0.193	-24.3 ± 0.1	N.D.	N.D.	N.D.

"The critical coagulation concentration is set as the first value corresponding to a sizable jump in the absorption ratio, as shown in Figure 3. The DLS measurements were carried out in DI water. The CCC values quantify the colloidal stability in NaCl, dithiothreitol (DTT), and amphiphile peptide (FFPC) assays. These assays screen for the favorable electrostatic, covalent, and $\pi - \pi$ stacking interactions between the AuNPs and aggregants, respectively. Indicates aggregation Not Detected under the tested conditions.

aggregating peptide. ¹⁶ The Derjaguin–Landau–Verwey–Overbeek (DLVO) theory stresses the balance of the van der Waals attractive force and electrostatic repulsive force on colloidal stability. ³⁵ Thus, NPs are more likely to aggregate upon reduction of the double-layer repulsion by (i) adding oppositely charged peptides and/or (ii) decreasing the surface potential. The latter is directly related to surface chemistry and thus impacts coagulation between NPs and peptides *via* electrostatic interactions.

Covalent dithiol-bridging and noncovalent $\pi-\pi$ stacking can also facilitate AuNP coagulation. 15,36,37 Typically, color changes prevail for AuNPs of compact ligand layers and in favorable particle-particle interacting environments. 27,28 Meanwhile, minimal or no optical change is observed for AuNPs capped by inert, entropic, and strong-coordinating ligands. 31,38,39 In this study, the effect of surface ligands on colorimetric assays was investigated using 19 ligand-metal nanocomposites comprising 13-nm AuNPs (see TEM in Figure S1). Aggregation was evaluated using a proteasecleavable peptide that is flanked by segments with Arg, Cys, and Phe amino acids, as shown in Figure 1a. Figure 1b shows the chemical structures of the ligands included here. These molecules represent different molecular weights, charges (neutral or anionic for the compatibility with citrate-AuNPs), and coordination strengths, thus evaluating a wide range of colloidal stability on nanoparticles.

2.2. Ligand Library and Characterization of AuNPs. Despite a combination of molecular forces involved in ligand-to-metal interactions, we simplified our discussion and grouped these ligands based on the hard—soft acid—base (HSAB) theory where the Au atom receptor on nanosurfaces is classified as a soft Lewis acid. The hard base-type ligands have characteristic anchors such as hydroxyl, carboxylate (or carboxyl), and sulfonate groups, which are expected to be labile molecules and weakly passivate Au nanosurfaces; examples

include citrate, polyphenols [i.e., (-)-epigallocatechin gallate (EGCG), tannic acid (TA)], and labile-binding macromolecules [i.e., poly(acrylic acid) (PAA), poly(sodium 4styrenesulfonate) (PSS), poly(vinylpyrrolidone) (PVP)].42 The soft base-type ligands tethered with thiol (Au-S strength \approx 126–184 kJ/mol⁴³), phosphine (Au–P strength \approx 222 kJ/ mol⁴⁴), or carbon (Au-C strength ≈ 227 kJ/mol⁴⁵) anchors are known for strongly coordinating on AuNPs and thus favoring colloidal stabilization; examples include phosphine ligands [i.e., tris(2-carboxyethyl)phosphine (TCEP), (diphenylphosphino)benzene sulfonate (DPPS), bis(psulfonatophenyl)phenylphosphine (BSPP)], thiolate ligands [i.e., dithiothreitol (DTT), mercaptopropionic acid (MPA), mercaptopropane sulfonate (MPS), reduced glutathione (GSH), thiolate carboxyl-poly(ethylene glycol) (HS-PEG-COOH), lipoic acid-zwitterion (LA-ZW), lipoic acid-terminated carboxyl-poly(ethylene glycol) (LA-PEG-COOH), poly-(isobutylene-alt-maleic anhydride) with LA and methoxy-PEG pendant groups (LA-PIMA-PEG)], and calix[4]arene (X₄C₄) molecules. 28,29,46,47 The ligand exchange protocol starting from citrate-AuNPs was performed according to a previous report with slight modifications. 29,38 Note that the MPS- and MPAcapped AuNPs were sequentially derived using BSPP-AuNPs as the intermediate. The X₄C₄ ligand is modified upon reduction and NP synthesis in situ without ligand exchange, and it is grafted through covalent Au-C bonds.40 The new ligand-capped AuNPs were characterized by dynamic light scattering (DLS) and zeta potential (ζ) measurements (Table 1). The larger hydrodynamic diameter (D_H) and polydispersity index (PDI) measured after ligand substitution indicate the more complex architecture of the new coatings than native citrate anions. 48 These measured DH values are consistent with our previous data collected for AuNPs prepared using similar methods.16

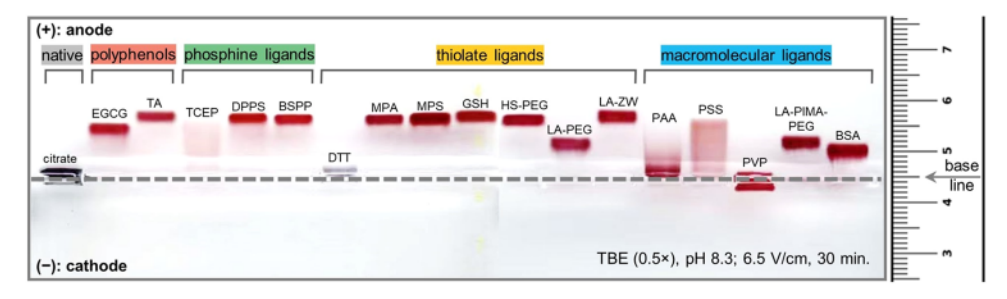


Figure 2. Agarose gel (0.7%) electrophoresis images collected from AuNPs capped with different ligands. Gel conditions are given in the bottom right, and the samples were prepared using a mixture of 3 μ L of glycerol and 47 μ L of AuNPs (10 nM). Note that tris-borate-EDTA buffer (TBE, 0.5×, pH 8.3) promotes instant aggregation of citrate- and DTT-capped AuNPs.

The above size characterization for the derivatized AuNPs was further corroborated by gel electrophoresis (Figure 2) due to the sensitivity of the electrophoretic mobility to subtle changes in the surface charge and hydrodynamic dimension. The citrate- and DTT-AuNPs showed instant aggregation in the running buffer (pH 8.3) and thus had no mobility shift. Most of the other NPs were stable enough to travel toward the anode, a property attributed to the hydroxyl/carboxylate/ sulfonate groups around the nanocrystal. For example, the polyphenol-, sulfonated phosphine-, and thiolate ligandscapped AuNPs exhibited sharp and narrow gel bands, indicating a low size dispersity. The TCEP-AuNPs showed a significant band smear implying moderate colloidal stabilitythis result is consistent with other reports and ours. 16,28 Meanwhile, AuNPs ligated with negatively charged polymers such as LA-PEG-COOH (990 Da), ⁵¹ PAA (15 kDa), PSS (70 kDa), LA-PIMA-PEG (25 kDa), ⁴⁸ and BSA (66 kDa) have retarded band shifts presumably due to the large size of the nanocomposites. A close look at the band of PAA-AuNPs and PSS-AuNPs indicates that these complexes were too large to travel in the gel pores and thus showed a long trailing tail.¹⁶ The PVP (40 kDa)-AuNP band showed no movement due to its charge neutrality. The above observations confirmed that ligand exchange on AuNPs with various ligands took place, and the derivatized AuNPs have distinct properties such as charge, size, and stability.

2.3. Colorimetric Tests under Excess lons, Thiols, and Aromatic Moieties. Next, evolution of the dispersion color and colloidal stability of the ligand-stabilized AuNPs (3.4 nM, 100 μ L) was evaluated in solutions containing NaCl (0–1 M), ^{28,49} DTT (0–100 μ M), ^{16,50} and amphiphilic peptides (*i.e.*, solubility of FFPC in water: 500 μ M). These assays screen for the favorable interparticle interactions (*e.g.*, electrostatic, covalent, and π – π stacking ^{38,49,52}) imparted by each ligand coating, and thus have important implications in designing peptides or other substrates for aggregation-based colorimetric assays. When the colloidal stability is compromised, the red color turns to purple/blue and finally to gray corresponding to higher aggregation levels.

In the first assay, charged AuNPs collapse with high levels of counterions due to the shortened Debye length and reduced electrostatic double-layer potential as described by the Schulze—Hardy rule.^{20,35,53} Figure 3a shows that NPs modified with compact and charged ligands, regardless of the anchoring groups, were prone to aggregation and showed color changes in high ionic strength conditions albeit at different thresholds of NaCl concentration.^{28,49} The quantitative assessment (*i.e.*, ratio at Abs₆₀₀/Abs₅₂₀) is shown in Figure 3d, and the CCC (defined as the first concentration of signal jump⁵⁴) is

summarized in Table 1. The clinically relevant level for sodium is about 140 mM at which point citrate-, TA-, TCEP-, DTT-, MPA-, MPS-, and PSS-capped AuNPs showed color changes and thus may suffer from background interference in clinical samples. AuNPs protected by EGCG, DPPS, BSPP, GSH, X₄C₄, and PAA molecules were more resistant to the ionic environment and produced color changes only when the salt concentration exceeds 200 mM, thus implying that they are good candidates for electrostatic-induced plasmonic coupling. In comparison, ligands appended with PEG blocks or zwitterionic motifs are expectedly less sensitive to ionic strength and retained the colloidal stability of AuNPs throughout the tested conditions.²⁹ The ζ potential can provide valuable information for predicting colloidal stability during charge screening tests, but its value must be weighted relative to other factors such as ligand size and binding strength, 38,49 which can also impact the CCC values as shown in Table 1.

In the second case, DTT molecules show high affinity to gold surfaces and competitively displace labile ligands, thus favoring chemical crosslinking and plasmonic coupling. 16,50 The covalent aggregation is promoted in ionic conditions (*i.e.*, 10 mM of NaCl) because of added screening effects; note that all of the AuNPs were stable in 10 mM NaCl. Figure 3b shows that citrate-, TA-, TCEP-, PAA-, and PSS-capped AuNPs (mostly hard Lewis base-anchoring groups) agglomerated in the DTT test: These gold dispersions rapidly changed colors at low amounts of DTT (*e.g.*, 5–20 μ M), while the same nanoparticles were stabilized at high concentrations probably due to the replacement of the native ligands by DTT and saturation of the particle surfaces.

The ratiometric absorbance data at various DTT concentrations for each AuNP type are summarized in Figure 3e and Table 1. The sulfonated phosphine (i.e., DPPS, BSPP)-coated AuNPs were resistant to DTT aggregation for hours, which may be attributed to the steric hindrance from the bulky aromatic rings that impedes ligand substitution. In addition, the nanoparticles functionalized with labile polymers (i.e., PAA and PSS) exhibited narrow aggregation windows (i.e., 5–10 μ M). As expected, AuNPs modified with high densities of thiolate ligands were insensitive to the DTT assay.

In the third scenario, increasing interfacial hydrophobicity destabilizes nanoparticles in aqueous media *via* solvophobic interactions, thus promoting their self-assembly and plasmonic coupling.³⁶ The FFPC peptide is a unique, compact, and neutral amphiphile simultaneously exhibiting good water solubility (from Pro), ^{24,55} aromaticity (from Phe), ⁵² and surface affinity (from Cys). ³⁶ The inclusion of the Cys sulfhydryl localizes aromatic interactions at bio-nano interfaces,

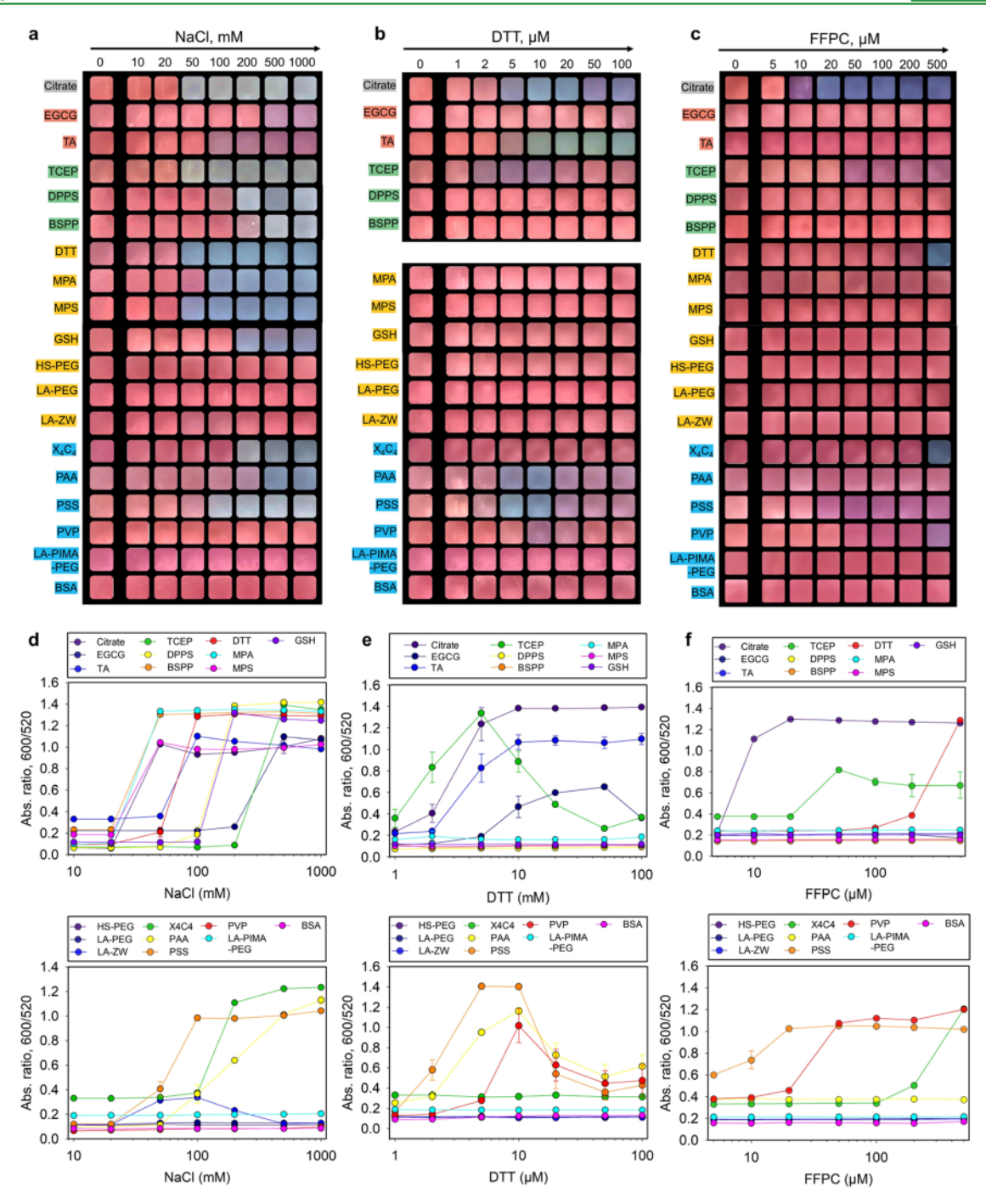


Figure 3. (a–c) Color patterns of the ligated AuNPs (3.4 nM, 100 μ L) in a series of NaCl, dithiothreitol (DTT), and amphiphilic peptide (FFPC) solutions of increasing concentrations (pH ~8.0). Shown are the cropped images at 10 min incubation. Red indicates dispersed nanoparticles. Purple, blue, and gray indicate increasing aggregation levels. The color pattern of DTT-AuNPs under DTT test is not included due to low reproducibility. (d–f) Quantitative analysis of the color patterns by measuring the ratiometric absorbance, Abs₆₀₀/Abs₅₂₀. The critical coagulation concentration (CCC) is defined as the first point of signal jump, where the ratiometric absorbance may vary. Error bars = standard deviations (n = 3). Panel (b) is reprinted with permission from ref 16. Copyright 2022 American Chemical Society.

which promotes mass-driven ligand exchange and AuNP aggregation in aqueous media. These unique properties make the FFPC peptide suitable for screening coatings that favor color changes $via \pi - \pi$ stacking. Citrate-, TCEP-, DTT-, X_4C_4 -, and PSS-AuNPs aggregated in the solution of FFPC (Figure 3c). The corresponding CCC is shown in Figure 3f and Table 1. This result agrees well with the above DTT test assuming that both assays require competitive displacement of the native ligands to initiate particle aggregation. Surprisingly, X_4C_4 -

AuNPs stabilized by covalent Au–C bond showed dramatic particle agglomeration at 500 μ M of FFPC peptide. It may be due to the fact that the $\rm X_4C_4$ ligands are strongly grafted at the surface and thus could not reorganize as thiols in self-assembled monolayers, leaving some gold surface available for sequestering thiols. The FFPC peptide being longer than DTT can protrude from the $\rm X_4C_4$ layer and render the particle coating more hydrophobic, leading to their aggregation. Figures S3–S5 details all of the spectroscopic evolution of

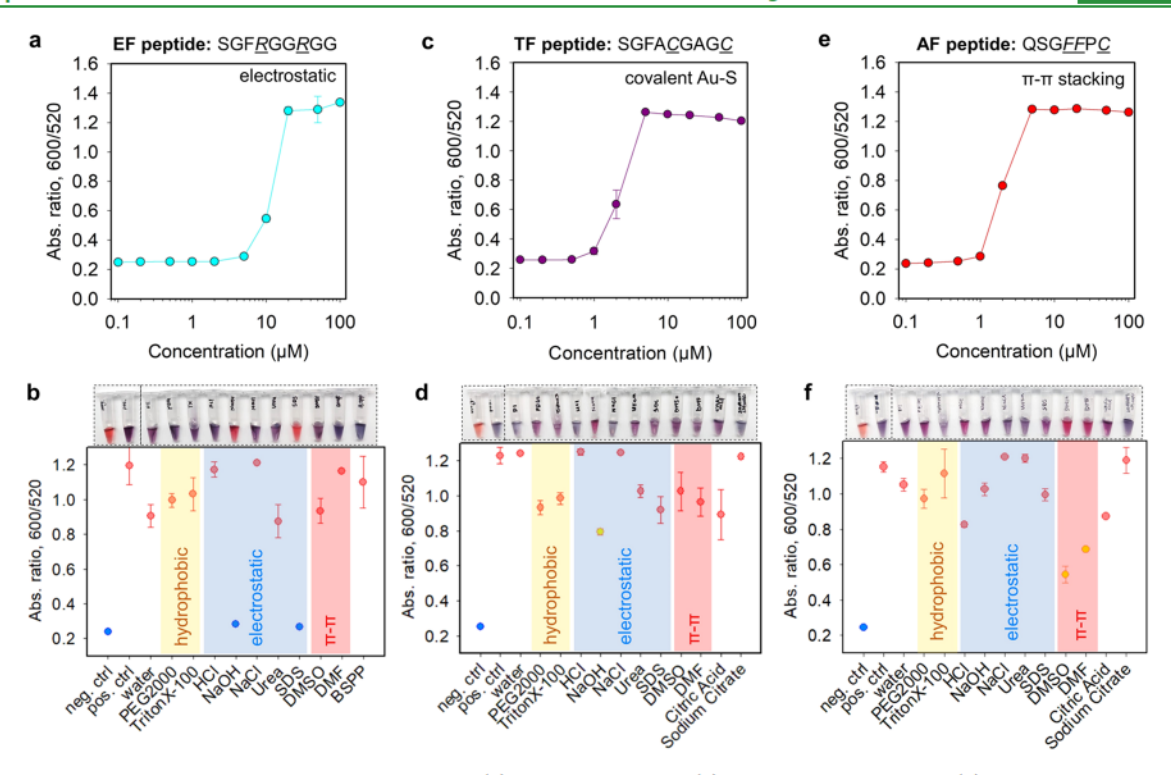


Figure 4. Aggregation titration of the representative paired (a) EF/BSPP-AuNPs, (c) TF/citrate-AuNPs, and (e) AF/citrate-AuNPs where the critical coagulation concentrations were determined to be about 10, 2, and 2 μ M, respectively. EF = electrostatic fragment; TF = thiolate fragment; and AF = aromatic fragment. (b, d, f) White-light image (top) and quantified reversal color change (bottom) of the peptide/AuNP aggregates in different surfactant solutions (10 mM, 100 μ L) or solvents (100 μ L). Negative control used the AuNPs only, and positive control used the peptide/AuNP aggregates only. The yellow area indicates dominant hydrophobic interactions, the blue area indicates prevalent electrostatic interactions, and the red area implies strong π – π stacking forces. Error bars = standard deviations (n = 3).

Table 2. Peptide and Segment Informationa

name	sequence ^b	M. W. (g/mol)	enzyme	description
EF	SGFRGGRGG-Am	848.43	N/A	two Arg, +2 charge
TF	SGFACGAGC-Am	770.28	N/A	two Cys, dithiol bridge
AF	SGFFPC-Am	655.28	N/A	two Phe, aromatic moiety
Mega	DDDTSAVLQ\SGFFRCRPC-Am	2014.90	$\mathbf{M}^{\mathrm{pro}}$	Zwitterionic, dithiolate, and aromatic substrate

^aThe electrostatic fragment (EF), thiolate fragment (TF), and aromatic fragment (AF) could induce aggregation of the AuNPs *via* electrostatic, covalent, and $\pi - \pi$ interactions, respectively. The Mega peptide after proteolysis can trigger AuNP aggregation *via* these multiple interactions. ^bAll peptides have a free N-terminus (*i.e.*, uncharged –NH₂ at pH 8.0) and an amidated C-terminus (*i.e.*, -Am). ↓ designates the M^{pro} cleavage site.

each AuNP sample in the above NaCl, DTT, and FFPC assays indicating a decrease in the SPR peak along with an increase in the absorbance at longer wavelengths.

2.4. Aggregation Assays with Peptides. Inspired by the above aggregation strategies, the charge/affinity/amphiphilicity of a specific substrate can be fine-tuned for colorimetric sensing of proteases where a diverse set of chemical functions provided by the aliphatic, protic, polar, aromatic amino acid side chains, and combinations thereof enable a versatile peptide library of distinct physicochemical properties. The selectivity is based on molecular recognition between the protease and the programmed peptide. Here, we selected SARS-CoV-2 Mpro to report on three sets of AuNP-aggregating peptide segments (see Figure 4 and Table 2); M^{pro} is known to effectively cleave at the C-terminal of Gln (Q) in the AVLQ1 SGF sequence.⁵⁶ The first peptide used electrostatic fragment (referred to as EF): two Arg (R) were positioned near the Nterminus for promoting electrostatic interactions, i.e., SGFRGGRGG.²⁵ The second peptide used thiolate fragment (referred to as TF), and two Cys (C) were coded to aggregate

AuNPs *via* covalent bonding, *i.e.*, <u>SGF</u>ACGAGC. The third peptide used aromatic fragment (referred to as AF), and two Phe (F) were incorporated to promote AuNP aggregation through $\pi-\pi$ stacking interactions, *i.e.*, <u>SGF</u>FPC. Note that these peptide segments retain the <u>SGF</u> sequence to mimic the M^{pro} cleavage site and contain a spacer sequence using Gly (G), Ala (A), and/or Pro (P). The peptide synthesis has been confirmed by HPLC and ESI-MS data (Figure S6).

Next, the 19 types of ligated AuNPs were titrated with 0–100 μ M of the above peptide segments, and the representative time-dependent aggregation kinetics are shown in Figure S7. The results at 10 min readout time were analyzed to pursue a rapid detection (Figure S8). The types of ligated AuNPs aggregated by the EF, TF, and AF peptides agree with the results from the above NaCl, DTT, and FFPC tests. This is because the peptides were customized to mimic the properties of these simple chemicals and thus the same interplay between the coating and peptide segment.

The Arg-rich EF segment agglomerated AuNPs coated with citrate, polyphenols, phosphine, DTT, MPA, MPS, X₄C₄, PAA,

Table 3. Critical Coagulation Concentration (CCC) of Various Ligated AuNPs with Three Segments^a

ligand type	sample	EF (μM)	TF (μM)	AF (μM)
native	citrate-Au	1	2	2
polyphenols	EGCG-Au	20	N.D. ^b	N.D.
	TA-Au	20	50	N.D.
phosphine ligands	TCEP-Au	0.5	5	N.D.
	DPPS-Au	5	50	100
	BSPP-Au	10	N.D.	N.D.
thiolate ligands	DTT-Au	1	50	N.D.
	MPA-Au	5	50	50
	MPS-Au	10	50	N.D.
	GSH-Au	50	50	N.D.
	HS-PEG _{∼110} -COOH-Au	50	100	N.D.
	LA-PEG ₁₂ -COOH-Au	N.D.	50	N.D.
	LA-ZW-Au	50	50	N.D.
macromolecular ligands	X_4C_4 -Au	20	N.D.	N.D.
	PAA-Au	5	N.D.	N.D.
	PSS-Au	0.5	10	5
	PVP-Au	2	10	5
	LA-PIMA-PEG ₁₅ -Au	N.D.	N.D.	N.D.
	BSA-Au	N.D.	N.D.	N.D.

^aThe aggregation induced by electrostatic fragment (EF), thiolate fragment (TF), and aromatic fragment (AF) is through electrostatic, covalent, and $\pi - \pi$ stacking interaction, respectively. ^{ba}N.D." indicates NP aggregation Not Detected under the tested conditions.

and PSS ligand. The charge-based aggregation depends on two aspects: (i) charge valence (Z) of counterions that follows the Schulz–Hardy rule and (ii) colloidal stability that follows the DLVO theory.³⁵

In the first aspect of electrostatic-based aggregation, the corresponding CCC values for each ligated AuNP with EF peptide are 4 orders of magnitude lower than that with NaCl (i.e., observed 10,000-fold less, see Table 1 versus 3). This discrepancy broadly follows the Schulz-Hardy rule (i.e., CCC $\propto Z^6$, theoretically 64-fold less), where the charge valence in an EF segment is twice as higher as a simple Na+ and thus less EF is required to electrostatically attract oppositely charged NPs. The different observed and theoretical values could result from the distinct ion geometries for different ions of the same valence,⁵⁷ e.g., Arg guanidinium allows interactions in three possible directions with the anionic counterparts through its three asymmetrical nitrogen atoms, compared to the Na⁺. On the one hand, these findings imply that the Arg-rich EF segment could be replaced with other substrates with positively charged side chains (e.g., Lys amino or His imidazole) to achieve the same purpose but at much higher concentrations or valences. On the other hand, increasing the charge valence of substrate can effectively reduce the CCC and enhance probe sensitivity with a plateau reached at valence of 2 or 3 due to an intrinsic trade-off in the sensor working window (i.e., a set of peptide concentrations where the color pattern differs before/ after proteolysis).53

In the second aspect of electrostatic-based aggregation, BSPP and DPPS ligands are structurally similar and are differentiated by their number of sulfonates (see structures in Figure 1b), where the measured ζ potential is -31.3 ± 1.8 and $-25.2\pm0.3\,$ mV, respectively. Typically, highly charged nanoparticles have strong electrostatic repulsion, reduced van der Waals attraction, long Debye lengths, and thus good colloidal stability. That is, BSPP-AuNPs would be less sensitive than DPPS-AuNPs upon counterion titration, e.g., the CCC of DPPS-AuNPs and BSPP-AuNPs in the presence of NaCl is 50 and 100 mM, respectively, and the CCC of DPPS-AuNPs and

BSPP-AuNPs in the presence of EF is 5 and 10 μ M, respectively (Tables 1,3). Experimentally, BSPP-AuNPs were more resistant to charge-induced aggregation, thus giving rise to a wide working window for good sensor performance with less background interference, albeit with a minor compromised sensitivity (Figure S9a,b). To summarize, the choice of a peptide/AuNP pair as a good color sensor is determined by the charge valence of counterions and the matched colloidal stability, e.g., low charge valence shall be paired with weak stability or vice versa (Figure S9).

To better understand the interparticle interactions, reversibility experiments were carried out for the EF peptide/BSPP-AuNPs aggregates employing several solvents and surfactants (10 mM). In Figure 4a,b, the gold pellet (3.4 nM, 100 μ L) freshly clustered by EF peptide (1.62 mM, 2.4 μ L) readily disassociated and returned to red in the presence of sodium dodecyl sulfate (SDS). The excess anionic SDS scavenges the positively charged EF peptides, thus restoring the electrostatic double-layer repulsions between particles. In addition, shifting the pH to 11 also fully recovered the BSPP-AuNPs, which is likely due to (i) the deprotonation of the guanidinium ions and restoration of the electrostatic repulsion between nanoparticles and/or (ii) high concentration of OH⁻ that deprotonates the native citrate residues under basic conditions, thus leading to interparticle electrostatic repulsions.

The TF peptide contains a divalent-Cys and bridges AuNPs capped with citrate, TCEP, PVP, and PSS molecules. Here, the determined CCC values are in the same range compared to that of DTT-induced aggregation (Tables 1 and 3). For instance, both TF peptide and DTT triggered instant color changes on citrate-AuNPs in the range of $2-5~\mu M$ or more (Figure 4c). This range is lower than a previously reported value because of the different fractions of thiolate segments in the solution (here, $\sim 100\%$ purity, Figure S6). Notably, the TF peptide could not aggregate DPPS- or BSPP-AuNPs within 1 h despite Au-S being stronger than Au-P bonds, which agrees well with the data shown for DTT test above (Figure 3b). Thiolate ligand-capped AuNPs were insensitive to TF

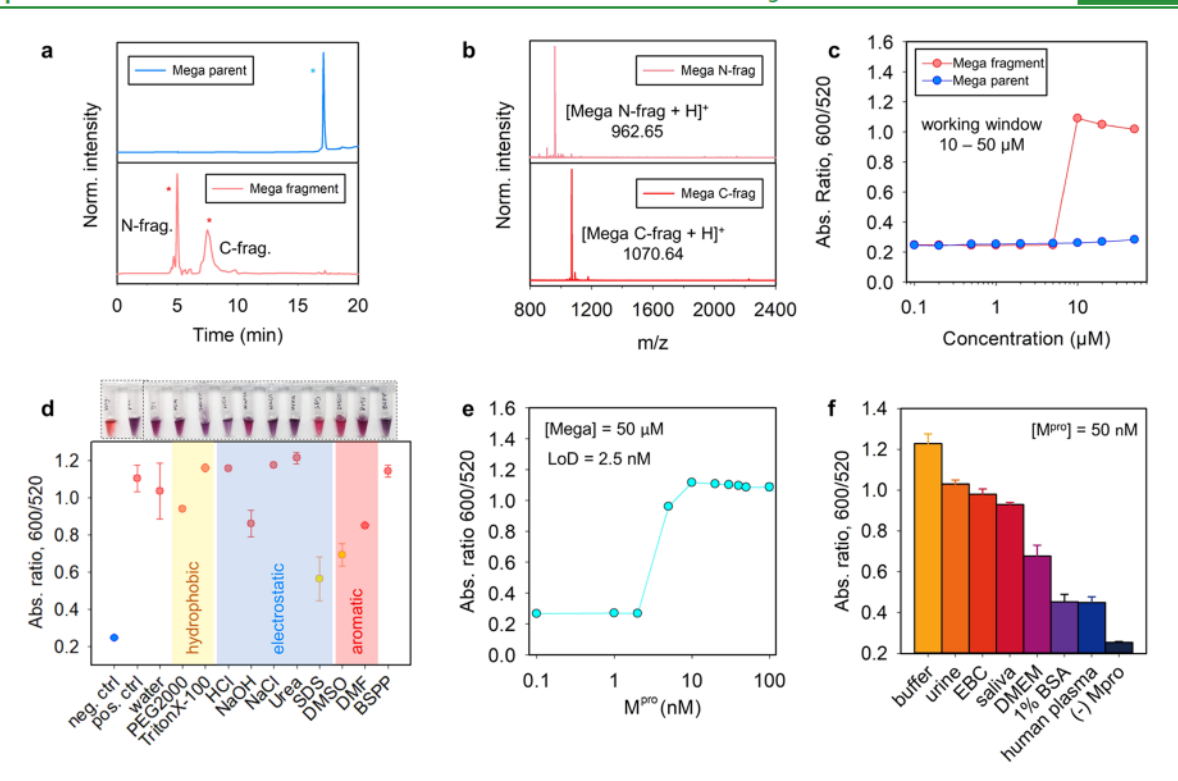


Figure 5. Improved performance of Mega peptide in colorimetric sensor. (a, b) HPLC and ESI-MS data confirm that M^{pro} cleaves the Mega peptide between Q and S. Peaks with * are the intact peptide (blue); the fragments are in red. (c) Ratiometric signal (Abs_{600}/Abs_{520} at 10 min readout time) recorded from BSPP-AuNPs (3.4 nM, 100 μ L) incubated with various amounts of intact Mega (red) and the fragments (blue). (d) White-light image (top) and quantified reversal color change (bottom) of the Mega/AuNP pellet in different surfactant solutions (10 mM, 100 μ L) or solvents (100 μ L). The redispersion in an SDS solution and DMSO solvent indicates dominant electrostatic and aromatic forces with scarce covalent bonding. (e) Ratiometric absorbance as a function of M^{pro} concentration. Conditions used the Mega substrate (100 μ M), BSPP-AuNPs (3.4 nM), and a 10 min assay time. The determined limit of detection is 2.5 nM in Tris buffer. (f) Sensor performance in other biological media. Positive control used the buffer with M^{pro} (100 nM), and negative control used the buffer without M^{pro} . Error bar = standard deviation (n = 3).

peptide titration. However, unlike the DTT molecule the TF peptide did not show stabilizing effect for AuNPs at high concentrations. Of note, we have previously reported that the tetravalent-Cys peptide did not improve the sensor performance rather compromise the working window due to dangling and reactive sulfhydryl undermining the overall colloidal stability when appended with a stabilizing moiety. ¹⁶ In Figure 4d, the aggregation based on covalent coupling was also validated using the same reversibility experiments, where the gold pellet (3.4 nM, 100 μ L, citrate-AuNPs) freshly clustered by TF peptide (980 μ M, 1 μ L) could not be redispersed in any of the surfactants/solvents employed.

The Phe-rich AF peptide aggregates AuNPs coated with citrate, PVP, and PSS molecules, and the CCC values are summarized in Table 3. In a previous work, we found that at the minimum, Phe-Phe was needed to induce π – π stacking while a single Phe only yielded hydrophobic interactions. In addition, the AF peptide without a Cys residue could not directly bridge aromatic ligands (e.g., DPPS and TA) via π -stacking, which is likely uncoupled by the hydration layer initiated by the ligands. That is, the AF peptide could also aggregate AuNPs capped with ligands that do not display any aromatic moiety (i.e., citrate, PVP, and PSS). In Figure 4f, the purple gold pellet (3.4 nM, 100 μ L) clustered by AF peptide (6.2 mM, 10 μ L) could be redispersed to red in organic solvents including dimethyl sulfoxide (DMSO) and dimethylformamide (DMF). This indicates prevalent π – π interactions in the AF peptide/AuNP pellet. As such, the design of AF

eliminates the concerns of peptide functional loss in complex milieu due to oxidation and charge scavengers.

The redispersion of peptide/AuNP aggregates reveals the critical role of Arg/Cys/Phe residues, which govern the interplays among nanoparticles of a specific coating. Overall, the EF peptide crosslinks AuNPs capped with compact and charged ligands such as TA, DPPS, BSPP, or X_4C_4 molecules. Nonetheless, the EF peptide cannot associate NPs coated with charge-neutral ligands such as PVP, which could be clustered by the TF or AF peptide through covalent coupling or $\pi-\pi$ stacking interactions. In addition, the TF and AF peptides require a direct contact of the Cys sulfhydryl to the Au atom and thus cannot aggregate well-passivated surfaces including thiolate and sulfonated phosphine ligand AuNPs, while a few of these NPs strongly interact with the EF peptide due to the charged terminal groups.

2.5. Peptide Optimization and Protease Detection. Previous reports also stressed the limitations of aggregation-based colorimetric sensors under dynamic condition, e.g., the electrostatic attraction-governed systems were largely impeded in complex biological media such as saliva and human plasma due to the abundance of negatively charged proteins forming a protein corona and/or scavenging the aggregating counterions. In addition, the electrostatic interactions between the Arguanidine and ligand carboxylate were sensitive to the environmental pH because of protonation/deprotonation status. Efforts were input to improve the sensor performance using Cys-/Phe-coded substrates; nonetheless, these peptides may suffer from oxidative and ionic conditions due to the

requirement of reduced sulfhydryl and moderate surface passivation. ^{16,23} Therefore, combining all of these interparticle forces in one peptide substrate may expand the types of ligated AuNPs for use and retain the peptidic function under complex biological media.

The "Mega" peptide (DDDTSAVLQ\SGFFRCRPC, Table 2) was customized to encompass three functional domains composed of (i) an N-terminal stabilizing domain made of three Asp (DDD) for neutralizing the net charge of the substrate and minimizing interactions with NPs, (ii) a central M^{pro} cleavage site consisting of TSAVLQ\SGF, and (iii) a C-terminal destabilizing domain for aggregating colloidal gold (Figure 1a). The destabilizing domain has two Arg and Phe for promoting electrostatic and $\pi-\pi$ stacking interactions respectively, and two Cys for sequestering surface Au, thus promoting covalent interplay. Here, we hypothesize that proteolysis of the intact Mega peptide will lead to a strong aggregating segment and subsequently flocculate ligated AuNPs via a combination of interactions, thus producing intense color changes under various conditions.

Figure 5a shows the HPLC profiles of the synthetic Mega peptide before and after proteolysis by M^{pro}. Figure 5b indicates that the cleavage of Mega peptide liberated the SGFFRCRPC fragment (calcd. 1070.49; found, 1070.64). We first determined the working window for M^{pro} detection by recording the ratiometric absorbance (Abs₆₀₀/Abs₅₂₀ at 10 min) after the addition of AuNPs (3.4 nM, 100 μ L) to the parent and its fragments of varying concentrations (i.e., 0-50 μ M). We selected BSPP-AuNPs as a representative case for the sake of improved colloidal stability and good sensing performance. As shown in Figure 5c, the intact Mega peptide caused no NP aggregation at the tested concentrations. In comparison, addition of the fragments exceeding 5.0 μ M induced a noticeable color change in buffer and sizeable ratiometric absorbance signal. Thus, we defined $10-50 \mu M$ as the working window for the Mega peptide/BSPP-AuNPs pair. The working window of other combinations involving different surface coatings is provided in Figure S10, where the AuNPs capped with citrate, DPPS, BSPP, MPA, MPS, GSH, HS-PEG-COOH, LA-ZW, X₄C₄, and PSS showed good sensing values. The choices of AuNP type are enlarged for colorimetric sensors due to the strong aggregating propensity of the Mega segment that renders diverse interactions. Regardless of the various surface coatings, high concentrations of Mega peptide in the assay would benefit the probe sensitivity, and thus 50 µM was defined as the optimal substrate concentration for the next experiments.

The limit of detection (LoD) was then investigated by incubating the Mega peptide (50 μ M) with varying amounts of M^{pro} (0-100 nM) in Tris buffer (TB, 20 mM, pH 8.0) in a 20 µL assay volume for 3 h. Next, a dispersion of BSPP-AuNPs $(3.4 \text{ nM}, 100 \mu\text{L})$ was added as the color agent. Figure 5c shows the ratiometric signal as a function of Mpro concentration. Therefore, the LoD for Mpro was 2.5 nM in Tris buffer; analysis used a previously reported method.⁵⁴ Of note, M^{pro} has no effects on the stability of BSPP-AuNPs. The exact levels of the M^{pro} that are clinically relevant in respiratory fluids of COVID-19 patients still remain uncertain,⁵⁸ but our detection limit is about 5- to 20-fold more sensitive than previous reported colorimetric or fluorescent probes, e.g., previous NP-based colorimetric assays from our group relying on covalent, π – π stacking, and electrostatic interactions reported LoDs for M^{pro} about 10, 16, and 30 nM,

respectively. 16,25 Lin et al. also developed a peptide/AuNP system based on electrostatic interactions and reported an LoD of 10 nM.⁵⁹ Another related work using a fluorogenic substrate reported an LoD of 50 nM.60 Similarly, the commercial fluorogenic substrates (e.g., Covidyte EN450 substrate) typically detect M^{pro} as low as 20 nM. We attributed the improved detection limits to the strong aggregating propensity of the Mega segment, which contains Arg, Cys, and Phe, and thus renders versatile interparticle interplays including electrostatic, covalent, and aromatic interactions. This results in substantially lower amounts of fragment needed for initializing color changes. To this end, Figure 5d shows that the Mega peptide/BSPP-AuNP aggregates can be partially redispersed into an SDS solution and DMSO solvent, indicating prevalent π - π stacking and electrostatic interactions with a scarce covalent bonding, presumably the good surface passivation of BSPP ligands impeding the formation of two Au-S bonds on two different particles in a short period.

2.6. Matrix Effect. Next, we evaluated the matrix effects by first incubating the Mega peptide (50 μ M) with M^{pro} spiked in 20 μ L of different media for 3 h, such as TB (20 mM, pH 8.0), exhaled breath condensate (EBC), 1% bovine serum albumin (BSA) solution, human plasma, Dulbecco's modified Eagle's medium (DMEM), urine, and pooled human saliva. Subsequently, the BSPP-AuNP dispersion (3.4 nM, 100 μ L) was added to reach a 100 nM protease concentration, and the ratiometric absorbance at 10 min was recorded (Figure 5f). The Mega peptide/BSPP-AuNP showed good performance not only in TB and EBC but also in other complex media such as urine and pooled saliva. This is attributed to the complementary interparticle forces rendered by the Mega segments. This also indicates that enzymatic cleavage did occur in the matrixes and previous reports showing the quenched aggregations are most likely due to protein corona nonspecifically binding either the NPs or the released peptide segments. 24,61 For instance, EF peptide/BSPP-AuNP was limited in use in pooled saliva due to charge scavengers binding to the working peptide segments, 24,25 and the TF peptide/citrate-AuNPs showed no color change in human plasma presumably because the protein corona formation on the AuNPs. 16,23 Control assays showed that the BSPP-AuNPs were stable in the tested matrixes except human plasma (i.e., about 40% aggregation level in human plasma only, Figure S11).49

Finally, we would like to note that (i) the present multifactorial design does not hold surface coverage constant and (ii) the aggregation trend may not extrapolate to other NP compositions/morphologies.^{3,62} We emphasize that this study used a large excess of ligand during the ligand exchange and thus ensured maximum surface coverage. 63 (iii) The size of the NPs could also impact the results: Large AuNPs with the same coating might have weaker stability and thus lower CCC due to compromised entropy stabilization (from ligands) relative to van der Waals affinity (from NPs). 29,39 Larger NPs also have a higher absorption cross section and could produce intense color changes.²⁹ Thus, large NPs might lead to good sensitivity but a narrow working window or vice versa. (iv) We also could not exclude the possibility of a false positive result from off-site target of the Mega peptide by other enzymes (e.g., gingipains⁶⁴) in the pooled saliva assays. (v) DMEM cell growth media, 1% BSA solution, and human plasma still impeded the aggregation kinetics of the Mega peptide/BSPP-AuNP by more than 50% presumably because of high-level protein corona formation (Figure 5f). ⁴⁹ A previous report indicates that BSA at 0.2 μ M could build protein corona and thus have stabilization effect on citrate-AuNPs. ¹⁶ A dilution factor of 5 and 20 is required for 1% BSA and plasma, respectively, to achieve successful aggregation of BSPP-AuNPs upon mixing with M^{pro}-incubated Mega peptide (Figure S12).

3. CONCLUSIONS

AuNPs coated with 19 ligands ranging from labile molecules to multicoordinating macromolecules were used as colorimetric agents, and their performance in aggregation-based colorimetric assays for protease detection was evaluated. The surface coatings favoring electrostatic, covalent, and $\pi-\pi$ stacking interactions were optimized using three customized peptides. Our results showed that AuNPs coated with TA, DPPS, BSPP, or X₄C₄ ligands were the best for electrostatic-based aggregation. These ligands all have a low molecular weight, compact size, high charge valence, and a high degree of aromaticity. In addition, AuNPs coated with citrate or PVP were the best for dithiol-induced and $\pi - \pi$ stacking interactionbased aggregation. These ligands generally have hard Lewis base-anchoring groups and thus weak binding strength. We also provided the rationale for peptide-based interactions in terms of side chain type and number, e.g., the good performance of electrostatic-based sensors requires aggregating peptides of low charge valence to be paired with charged NPs of weak stability or vice versa. We then designed and tested a combination of the so-called Mega peptide and BSPP-AuNPs as an optimized colorimetric sensor where the aggregation is driven by both electrostatic and aromatic forces. By quantifying the color change with measurable ratiometric absorbance, we have determined the LoD was 2.5 nM for Mpro. This sensor performs well not only in buffer and EBC but also in complex biological samples such as saliva and urine.

ASSOCIATED CONTENT

Supporting Information

The Supporting Information is available free of charge at https://pubs.acs.org/doi/10.1021/acsami.3c00862.

Materials, instrumentation, mass spectroscopy, peptide synthesis, AuNP synthesis, ligand exchange, gel electrophoresis, TEM, aggregation assays, working window, and matrices test control (PDF)

AUTHOR INFORMATION

Corresponding Author

Jesse V. Jokerst — Department of NanoEngineering, Materials Science and Engineering Program, and Department of Radiology, University of California, San Diego, La Jolla, California 92093, United States; ⊙ orcid.org/0000-0003-2829-6408; Email: jjokerst@ucsd.edu

Authors

Zhicheng Jin — Department of NanoEngineering, University of California, San Diego, La Jolla, California 92093, United States; Occid.org/0000-0001-6072-7533

Justin Yeung — Department of Bioengineering, University of California San Diego, La Jolla, California 92093, United States; © orcid.org/0000-0001-8615-5895

Jiajing Zhou — Department of NanoEngineering, University of California, San Diego, La Jolla, California 92093, United States; Orcid.org/0000-0001-5203-4737

Maurice Retout — Department of NanoEngineering, University of California, San Diego, La Jolla, California 92093, United States; occid.org/0000-0002-8140-6621

Wonjun Yim — Materials Science and Engineering Program, University of California, San Diego, La Jolla, California 92093, United States; orcid.org/0000-0002-0242-7898

Pavla Fajtová – Skaggs School of Pharmacy and Pharmaceutical Sciences, University of California, San Diego, La Jolla, California 92093, United States

Bryan Gosselin – Laboratoire de Chimie Organique, Université libre de Bruxelles (ULB), B-1050 Brussels, Belgium; Engineering of Molecular NanoSystems, Ecole Polytechnique de Bruxelles, Université libre de Bruxelles (ULB), B-1050 Brussels, Belgium

Ivan Jabin – Laboratoire de Chimie Organique, Université libre de Bruxelles (ULB), B-1050 Brussels, Belgium

Gilles Bruylants — Engineering of Molecular NanoSystems, Ecole Polytechnique de Bruxelles, Université libre de Bruxelles (ULB), B-1050 Brussels, Belgium; orcid.org/0000-0003-1752-5826

Hedi Mattoussi — Department of Chemistry and Biochemistry, Florida State University, Tallahassee, Florida 32306, United States; orcid.org/0000-0002-6511-9323

Anthony J. O'Donoghue — Skaggs School of Pharmacy and Pharmaceutical Sciences, University of California, San Diego, La Jolla, California 92093, United States

Complete contact information is available at: https://pubs.acs.org/10.1021/acsami.3c00862

Author Contributions

Z.J. and J.Y. contributed equally to this work.

Notes

The authors declare no competing financial interest.

ACKNOWLEDGMENTS

The authors thank the National Institutes of Health (R01 DE031114; R21 AG065776-S1; R21 AI157957) for financial support. M.R. acknowledges the Wallonie-Bruxelles International (WBI) of the Fédération Wallonie-Bruxelles for financial support. H.M. thanks the National Science Foundation (NSF-CHE, Grant #2005079) and AFOSR (Grant No. FA9550-18-1-0144).

ABBREVIATIONS

DTT, dithiothreitol CCC, critical coagulation concentration M^{pro}, main protease FFPC, Phe-Phe-Pro-Cys peptide EF, electrostatic fragment TF, thiolate fragment AF, aromatic fragment EGCG, (-)-epigallocatechin gallate TA, tannic acid PAA, poly(acrylic acid) PSS, poly(sodium 4-styrenesulfonate) PVP, polyvinylpyrrolidone TCEP, tris(2-carboxyethyl)phosphine DPPS, (diphenylphosphino)benzene sulfonate BSPP, bis(*p*-sulfonatophenyl)phenylphosphine MPA, mercaptopropionic acid MPS, mercaptopropane sulfonate GSH, reduced glutathione

- $HS-PEG_{\sim 110}$ -COOH, thiolate carboxyl-poly(ethylene glycol)
- LA-ZW, lipoic acid zwitterion
- LA-PE G_{12} -COOH, lipoic acid carboxyl-poly(ethylene glycol)
- LA-PIMA-PEG₁₅, lipoic acid poly(isobutylene-*alt*-maleic anhydride) appended with methoxy-PEG
- X_4C_4 , calix[4]arene
- TB, tris buffer
- EBC, exhaled breath condensate

REFERENCES

- (1) Grzelczak, M.; Liz-Marzán, L. M.; Klajn, R. Stimuli-responsive Self-assembly of Nanoparticles. *Chem. Soc. Rev.* 2019, 48, 1342–1361.
- (2) Song, M.; Wang, D.; Peana, S.; Choudhury, S.; Nyga, P.; Kudyshev, Z. A.; Yu, H.; Boltasseva, A.; Shalaev, V. M.; Kildishev, A. V. Colors with Plasmonic Nanostructures: A Full-spectrum Review. *Appl. Phys. Rev.* 2019, 6, No. 041308.
- (3) Chen, P.; Liu, X.; Goyal, G.; Tran, N. T.; Shing Ho, J. C.; Wang, Y.; Aili, D.; Liedberg, B. Nanoplasmonic Sensing from the Human Vision Perspective. *Anal. Chem.* 2018, *90*, 4916–4924.
- (4) Zeng, J.; Zhang, Y.; Zeng, T.; Aleisa, R.; Qiu, Z.; Chen, Y.; Huang, J.; Wang, D.; Yan, Z.; Yin, Y. Anisotropic Plasmonic Nanostructures for Colorimetric Sensing. *Nano Today* 2020, 32, No. 100855.
- (5) Retout, M.; Mantri, Y.; Jin, Z.; Zhou, J.; Noël, G.; Donovan, B.; Yim, W.; Jokerst, J. V. Peptide-Induced Fractal Assembly of Silver Nanoparticles for Visual Detection of Disease Biomarkers. *ACS Nano* 2022, *16*, 6165–6175.
- (6) Retout, M.; Jin, Z.; Tsujimoto, J.; Mantri, Y.; Borum, R.; Creyer, M. N.; Yim, W.; He, T.; Chang, Y.-C.; Jokerst, J. V. Di-Arginine Additives for Dissociation of Gold Nanoparticle Aggregates: A Matrix-Insensitive Approach with Applications in Protease Detection. ACS Appl. Mater. Interfaces 2022, 14, 52553–52565.
- (7) Heuer-Jungemann, A.; Feliu, N.; Bakaimi, I.; Hamaly, M.; Alkilany, A.; Chakraborty, I.; Masood, A.; Casula, M. F.; Kostopoulou, A.; Oh, E.; Susumu, K.; Stewart, M. H.; Medintz, I. L.; Stratakis, E.; Parak, W. J.; Kanaras, A. G. The Role of Ligands in the Chemical Synthesis and Applications of Inorganic Nanoparticles. *Chem. Rev.* 2019, 119, 4819—4880.
- (8) Jain, V.; Roy, S.; Roy, P.; Pillai, P. P. When Design Meets Function: The Prodigious Role of Surface Ligands in Regulating Nanoparticle Chemistry. *Chem. Mater.* 2022, 34, 7579-7597.
- (9) Saha, K.; Agasti, S. S.; Kim, C.; Li, X.; Rotello, V. M. Gold Nanoparticles in Chemical and Biological Sensing. *Chem. Rev.* 2012, 112, 2739–2779.
- (10) Zhou, W.; Gao, X.; Liu, D.; Chen, X. Gold Nanoparticles for In Vitro Diagnostics. Chem. Rev. 2015, 115, 10575-10636.
- (11) Howes, P. D.; Chandrawati, R.; Stevens, M. M. Colloidal Nanoparticles as Advanced Biological Sensors. *Science* 2014, 346, No. 1247390.
- (12) Polavarapu, L.; Pérez-Juste, J.; Xu, Q.-H.; Liz-Marzán, L. M. Optical Sensing of Biological, Chemical and Ionic Species through Aggregation of Plasmonic Nanoparticles. *J. Mater. Chem. C* 2014, 2, 7460–7476.
- (13) Aldewachi, H.; Chalati, T.; Woodroofe, M. N.; Bricklebank, N.; Sharrack, B.; Gardiner, P. Gold Nanoparticle-based Colorimetric Biosensors. *Nanoscale* **2018**, *10*, 18–33.
- (14) Alafeef, M.; Pan, D. Diagnostic Approaches For COVID-19: Lessons Learned and the Path Forward. ACS Nano 2022, 16, 11545—11576.
- (15) Guarise, C.; Pasquato, L.; De Filippis, V.; Scrimin, P. Gold Nanoparticles-based Protease Assay. *Proc. Natl. Acad. Sci. U.S.A.* 2006, 103, 3978–3982.
- (16) Jin, Z.; Yeung, J.; Zhou, J.; Cheng, Y.; Li, Y.; Mantri, Y.; He, T.; Yim, W.; Xu, M.; Wu, Z.; Fajtova, P.; Creyer, M. N.; Moore, C.; Fu, L.; Penny, W. F.; O'Donoghue, A. J.; Jokerst, J. V. Peptidic Sulfhydryl

- for Interfacing Nanocrystals and Subsequent Sensing of SARS-CoV-2 Protease. Chem. Mater. 2022, 34, 1259–1268.
- (17) Ye, D.; Shuhendler, A. J.; Cui, L.; Tong, L.; Tee, S. S.; Tikhomirov, G.; Felsher, D. W.; Rao, J. Bioorthogonal Cyclization-mediated *in situ* Self-assembly of Small-molecule Probes for Imaging Caspase Activity *in vivo. Nat. Chem.* 2014, 6, 519–526.
- (18) Mirkin, C. A.; Letsinger, R. L.; Mucic, R. C.; Storhoff, J. J. A DNA-based Method for Rationally Assembling Nanoparticles into Macroscopic Materials. *Nature* 1996, 382, 607–609.
- (19) Loynachan, C. N.; Soleimany, A. P.; Dudani, J. S.; Lin, Y.; Najer, A.; Bekdemir, A.; Chen, Q.; Bhatia, S. N.; Stevens, M. M. Renal Clearable Catalytic Gold Nanoclusters for *in vivo* Disease Monitoring. *Nat. Nanotechnol.* 2019, 14, 883–890.
- (20) Bian, T.; Gardin, A.; Gemen, J.; Houben, L.; Perego, C.; Lee, B.; Elad, N.; Chu, Z.; Pavan, G. M.; Klajn, R. Electrostatic Coassembly of Nanoparticles with Oppositely Charged Small Molecules into Static and Dynamic Superstructures. *Nat. Chem.* 2021, 13, 940–949.
- (21) Choueiri, R. M.; Klinkova, A.; Thérien-Aubin, Hs.; Rubinstein, M.; Kumacheva, E. Structural Transitions in Nanoparticle Assemblies Governed by Competing Nanoscale Forces. *J. Am. Chem. Soc.* 2013, 135, 10262–10265.
- (22) Kundu, P. K.; Samanta, D.; Leizrowice, R.; Margulis, B.; Zhao, H.; Börner, M.; Udayabhaskararao, T.; Manna, D.; Klajn, R. Lightcontrolled Self-assembly of Non-photoresponsive Nanoparticles. *Nat. Chem.* 2015, 7, 646–652.
- (23) Jin, Z.; Li, Y.; Li, K.; Zhou, J.; Yeung, J.; Ling, C.; Yim, W.; He, T.; Cheng, Y.; Xu, M.; Creyer, M. N.; Chang, Y.-C.; Fajtová, P.; Retout, M.; Qi, B.; Li, S.; O'Donoghue, A. J.; Jokerst, J. V. Peptide Amphiphile Mediated Co-assembly for Nanoplasmonic Sensing. *Angew. Chem.* 2023, 135, No. e202214394.
- (24) Jin, Z.; Ling, C.; Li, Y.; Zhou, J.; Li, K.; Yim, W.; Yeung, J.; Chang, Y.-C.; He, T.; Cheng, Y.; Fajtová, P.; Retout, M.; O'Donoghue, A. J.; Jokerst, J. V. Spacer Matters: All-Peptide-Based Ligand for Promoting Interfacial Proteolysis and Plasmonic Coupling. *Nano Lett.* 2022, 22, 8932–8940.
- (25) Jin, Z.; Mantri, Y.; Retout, M.; Cheng, Y.; Zhou, J.; Jorns, A.; Fajtova, P.; Yim, W.; Moore, C.; Xu, M.; Creyer, M. N.; Borum, R. M.; Zhou, J.; Wu, Z.; He, T.; Penny, W. F.; O'Donoghue, A. J.; Jokerst, J. V. A Charge-Switchable Zwitterionic Peptide for Rapid Detection of SARS-CoV-2 Main Protease. *Angew. Chem., Int. Ed.* 2022, 61, No. e202112995.
- (26) Creyer, M. N.; Jin, Z.; Moore, C.; Yim, W.; Zhou, J.; Jokerst, J. V. Modulation of Gold Nanorod Growth via the Proteolysis of Dithiol Peptides for Enzymatic Biomarker Detection. ACS Appl. Mater. Interfaces 2021, 13, 45236–45243.
- (27) Su, K. H.; Wei, Q. H.; Zhang, X.; Mock, J. J.; Smith, D. R.; Schultz, S. Interparticle Coupling Effects on Plasmon Resonances of Nanogold Particles. *Nano Lett.* 2003, 3, 1087–1090.
- (28) Wu, R.; Jiang, L.-P.; Zhu, J.-J.; Liu, J. Effects of Small Molecules on DNA Adsorption by Gold Nanoparticles and a Case Study of Tris(2-carboxyethyl)phosphine (TCEP). *Langmuir* 2019, 35, 13461–13468.
- (29) Jin, Z.; Sugiyama, Y.; Zhang, C.; Palui, G.; Xin, Y.; Du, L.; Wang, S.; Dridi, N.; Mattoussi, H. Rapid Photoligation of Gold Nanocolloids with Lipoic Acid-based Ligands. *Chem. Mater.* 2020, 32, 7469–7483.
- (30) Kovalenko, M. V.; Bodnarchuk, M. I.; Zaumseil, J.; Lee, J.-S.; Talapin, D. V. Expanding the Chemical Versatility of Colloidal Nanocrystals Capped with Molecular Metal Chalcogenide Ligands. *J. Am. Chem. Soc.* 2010, 132, 10085–10092.
- (31) Jokerst, J. V.; Lobovkina, T.; Zare, R. N.; Gambhir, S. S. Nanoparticle PEGylation for Imaging and Therapy. *Nanomedicine* 2011, 6, 715–728.
- (32) Palui, G.; Aldeek, F.; Wang, W.; Mattoussi, H. Strategies for Interfacing Inorganic Nanocrystals with Biological Systems based on Polymer-Coating. *Chem. Soc. Rev.* 2015, 44, 193–227.
- (33) Egorova, E. A.; van Rijt, M. M. J.; Sommerdijk, N.; Gooris, G. S.; Bouwstra, J. A.; Boyle, A. L.; Kros, A. One Peptide for Them All:

- Gold Nanoparticles of Different Sizes Are Stabilized by a Common Peptide Amphiphile. ACS Nano 2020, 14, 5874-5886.
- (34) Stordy, B.; Zhang, Y.; Sepahi, Z.; Khatami, M. H.; Kim, P. M.; Chan, W. C. W. Conjugating Ligands to an Equilibrated Nanoparticle Protein Corona Enables Cell Targeting in Serum. *Chem. Mater.* 2022, 34, 6868–6882.
- (35) Ohshima, H.The Derjaguin-Landau-Verwey-Overbeek (DLVO) Theory of Colloid Stability. In *Electrical Phenomena at Interfaces and Biointerfaces* 2012; pp 27–34 DOI: 10.1002/9781118135440.ch3.
- (36) Laromaine, A.; Koh, L.; Murugesan, M.; Ulijn, R. V.; Stevens, M. M. Protease-Triggered Dispersion of Nanoparticle Assemblies. *J. Am. Chem. Soc.* 2007, 129, 4156–4157.
- (37) Liu, X.; Zhang, Q.; Knoll, W.; Liedberg, B.; Wang, Y. Rational Design of Functional Peptide—Gold Hybrid Nanomaterials for Molecular Interactions. *Adv. Mater.* 2020, 32, No. 2000866.
- (38) Mei, B. C.; Oh, E.; Susumu, K.; Farrell, D.; Mountziaris, T. J.; Mattoussi, H. Effects of Ligand Coordination Number and Surface Curvature on the Stability of Gold Nanoparticles in Aqueous Solutions. *Langmuir* 2009, 25, 10604–10611.
- (39) Yang, Y.; Qin, H.; Jiang, M.; Lin, L.; Fu, T.; Dai, X.; Zhang, Z.; Niu, Y.; Cao, H.; Jin, Y.; Zhao, F.; Peng, X. Entropic Ligands for Nanocrystals: From Unexpected Solution Properties to Outstanding Processability. *Nano Lett.* 2016, 16, 2133–2138.
- (40) Troian-Gautier, L.; Mattiuzzi, A.; Reinaud, O.; Lagrost, C.; Jabin, I. Use of Calixarenes Bearing Diazonium Groups for the Development of Robust Monolayers with Unique Tailored Properties. *Org. Biomol. Chem.* 2020, 18, 3624–3637.
- (41) Pearson, R. G. Absolute Electronegativity and Hardness: Application to Inorganic Chemistry. *Inorg. Chem.* 1988, 27, 734–740.
- (42) Wu, D.; Zhou, J.; Creyer, M. N.; Yim, W.; Chen, Z.; Messersmith, P. B.; Jokerst, J. V. Phenolic-Enabled Nanotechnology: Versatile Particle Engineering for Biomedicine. *Chem. Soc. Rev.* 2021, 50, 4432–4483.
- (43) Häkkinen, H. The Gold-Sulfur Interface at the Nanoscale. *Nat. Chem.* 2012, 4, 443-455.
- (44) Borissova, A. O.; Korlyukov, A. A.; Antipin, M. Y.; Lyssenko, K. A. Estimation of Dissociation Energy in Donor—Acceptor Complex AuCl-PPh3 via Topological Analysis of the Experimental Electron Density Distribution Function. *J. Phys. Chem. A* 2008, 112, 11519—11522.
- (45) Antušek, A.; Blaško, M.; Urban, M.; Noga, P.; Kisić, D.; Nenadović, M.; Lončarević, D.; Rakočević, Z. Density Functional Theory Modeling of C-Au Chemical Bond Formation in Gold Implanted Polyethylene. *Phys. Chem. Chem. Phys.* 2017, 19, 28897—28906.
- (46) Tsai, D.-H.; Cho, T. J.; DelRio, F. W.; Gorham, J. M.; Zheng, J.; Tan, J.; Zachariah, M. R.; Hackley, V. A. Controlled Formation and Characterization of Dithiothreitol-Conjugated Gold Nanoparticle Clusters. *Langmuir* 2014, 30, 3397–3405.
- (47) Retout, M.; Jabin, I.; Bruylants, G. Synthesis of Ultrastable and Bioconjugable Ag, Au, and Bimetallic Ag_Au Nanoparticles Coated with Calix[4]arenes. ACS Omega 2021, 6, 19675–19684.
- (48) Zhang, C.; Jin, Z.; Zeng, B.; Wang, W.; Palui, G.; Mattoussi, H. Characterizing the Brownian Diffusion of Nanocolloids and Molecular Solutions: Diffusion-Ordered NMR Spectroscopy vs Dynamic Light Scattering. *J. Phys. Chem. B* 2020, 124, 4631–4650.
- (49) Johnston, B. D.; Kreyling, W. G.; Pfeiffer, C.; Schäffler, M.; Sarioglu, H.; Ristig, S.; Hirn, S.; Haberl, N.; Parak, W. J.; et al. Colloidal Stability and Surface Chemistry Are Key Factors for the Composition of the Protein Corona of Inorganic Gold Nanoparticles. *Adv. Funct. Mater.* 2017, 27, No. 1701956.
- (50) Mosquera, J.; García, I.; Henriksen-Lacey, M.; González-Rubio, G.; Liz-Marzán, L. M. Reducing Protein Corona Formation and Enhancing Colloidal Stability of Gold Nanoparticles by Capping with Silica Monolayers. *Chem. Mater.* 2019, 31, 57–61.
- (51) Susumu, K.; Mei, B. C.; Mattoussi, H. Multifunctional Ligands based on Dihydrolipoic Acid and Polyethylene Glycol to Promote Biocompatibility of Quantum Dots. *Nat. Protoc.* 2009, 4, 424–436.

- (52) Bera, S.; Mondal, S.; Xue, B.; Shimon, L. J. W.; Cao, Y.; Gazit, E. Rigid Helical-Like Assemblies from a Self-Aggregating Tripeptide. *Nat. Mater.* 2019, 18, 503-509.
- (53) Chang, Y.-C.; Jin, Z.; Li, K.; Zhou, J.; Yim, W.; Yeung, J.; Cheng, Y.; Retout, M.; Creyer, M. N.; Fajtová, P.; He, T.; Chen, X.; O'Donoghue, A. J.; Jokerst, J. V. Peptide Valence-Induced Breaks in Plasmonic Coupling. *Chem. Sci.* 2023, 14, 2659–2668.
- (54) Armbruster, D. A.; Pry, T. Limit of Blank, Limit of Detection and Limit of Quantitation. Clin. Biochem. Rev. 2008, 29, S49-S52.
- (55) Graham, B.; Bailey, T. L.; Healey, J. R. J.; Marcellini, M.; Deville, S.; Gibson, M. I. Polyproline as a Minimal Antifreeze Protein Mimic That Enhances the Cryopreservation of Cell Monolayers. *Angew. Chem., Int. Ed.* 2017, 56, 15941–15944.
- (56) Cheng, Y.; Borum, R. M.; Clark, A. E.; Jin, Z.; Moore, C.; Fajtová, P.; O'Donoghue, A. J.; Carlin, A. F.; Jokerst, J. V. A Dual-Color Fluorescent Probe Allows Simultaneous Imaging of Main and Papain-like Proteases of SARS-CoV-2-Infected Cells for Accurate Detection and Rapid Inhibitor Screening. *Angew. Chem., Int. Ed.* 2022, 61, No. e202113617.
- (57) Sokalingam, S.; Raghunathan, G.; Soundrarajan, N.; Lee, S.-G. A Study on the Effect of Surface Lysine to Arginine Mutagenesis on Protein Stability and Structure Using Green Fluorescent Protein. *PLoS One* **2012**, *7*, No. e40410.
- (58) Martínez-Fleta, P.; Alfranca, A.; González-Álvaro, I.; Casasnovas, J. M.; Fernández-Soto, D.; Esteso, G.; Cáceres-Martell, Y.; Gardeta, S.; López-Sanz, C.; Valés-Gómez, M. SARS-CoV-2 Cysteine-Like Protease Antibodies can be Detected in Serum and Saliva of COVID-19—Seropositive Individuals. *J. Immunol. Res.* 2020, 205, 3130—3140.
- (59) Feng, Y.; Liu, G.; La, M.; Liu, L. Colorimetric and Electrochemical Methods for the Detection of SARS-CoV-2 Main Protease by Peptide-Triggered Assembly of Gold Nanoparticles. *Molecules* 2022, 27, 615.
- (60) Moore, C.; Borum, R. M.; Mantri, Y.; Xu, M.; Fajtová, P.; O'Donoghue, A. J.; Jokerst, J. V. Activatable Carbocyanine Dimers for Photoacoustic and Fluorescent Detection of Protease Activity. *ACS Sens.* 2021, *6*, 2356–2365.
- (61) Vandooren, J.; Itoh, Y. Alpha-2-Macroglobulin in Inflammation, Immunity and Infections. *Front. Immunol.* 2021, *12*, No. 803244.
- (62) Wang, J.; Hsu, S.-w.; Gonzalez-Pech, N.; Jhunjhunwala, A.; Chen, F.; Hariri, A.; Grassian, V.; Tao, A.; Jokerst, J. V. Copper Sulfide Nanodisks and Nanoprisms for Photoacoustic Ovarian Tumor Imaging. *Part. Part. Syst. Charact.* 2019, 36, No. 1900171.
- (63) Jin, Z.; Kapur, A.; Wang, W.; Hernandez, J. D.; Thakur, M.; Mattoussi, H. The Dual—Function of Lipoic Acid Groups as Surface Anchors and Sulfhydryl Reactive Sites on Polymer—Stabilized QDs and Au Nanocolloids. *J. Chem. Phys.* 2019, 151, No. 164703.
- (64) Kaman, W. E.; Galassi, F.; de Soet, J. J.; Bizzarro, S.; Loos, B. G.; Veerman, E. C.; van Belkum, A.; Hays, J. P.; Bikker, F. J. Highly Specific Protease-Based Approach for Detection of Porphyromonas Gingivalis in Diagnosis of Periodontitis. *J. Clin. Microbiol.* 2012, 50, 104–112.